

Monte Carlo calculations of the AAPM Task Group 43
Dosimetry Parameters for the M-15 high dose rate
Iridium-192 brachytherapy source

April 30, 2014

Contents

1	Introduction	2
2	Materials and Methods	3
2.1	Brachytherapy source geometry and composition	3
2.2	Monte Carlo calculation techniques	4
3	Results and Discussion	6
3.1	Dose rate and normalized dose rate distribution	6
3.2	Geometry function, $\mathbf{G}_L(\mathbf{r}, \theta)$	9
3.3	Radial dose function, $\mathbf{g}_L(\mathbf{r})$	9
3.4	Anisotropy Function, $\mathbf{F}(\mathbf{r}, \theta)$, $\phi_{an}(\mathbf{r})$, and $\bar{\phi}_{an}$	11
3.5	$\dot{D}(\mathbf{r}_0, \theta_0)$, \mathbf{S}_k , and Λ	13
4	Conclusions	14
	Acknowledgment	14
	:	

Abstract

The Source Production & Equipment Co. (SPEC) Model M-15 Iridium Brachytherapy is intended for use as a temporary High Dose Rate (HDR) Brachytherapy source. The clinical dosimetry parameters of this source was calculated using the MCNP Monte Carlo analysis program (MCNP6; Los Alamos National Laboratory) in accordance to the updated AAPM Task Group Report No.43 (TG43U1). The parameters including S_k , $\dot{D}(r, \theta)$, Λ , $g_L(r)$, $F(r, \theta)$, $\phi_{an}(r)$, and $\bar{\phi}_{an}$ and their respective statistical uncertainty are presented in the reports.

1 Introduction

Iridium-192 , a standard high dose rate brachytherapy source, has been well studied and tested for clinical application in treatment of lung, esophageal, prostate, cervical, coronary, and other diseases.¹⁻⁵ Source Production & Equipment Co. (SPEC) has developed a new Iridium-192 high dose rate brachytherapy source, the Model M-15, for use in temporary High Dose Rate (HDR) Brachytherapy. In accordance with the recommendation of the updated AAPM Task Group Report No. 43 (TG43U1),⁶ this report performed a complete set of Monte Carlo calculations of the Model M-15 Iridium-192 Brachytherapy Source using the MCNP6 Monte Carlo code in both

water and air/vacuum modeled environments. The resulting dosimetric data was used to calculate the TG43U1 parameters. All derived quantities with their statistical uncertainties were calculated and are presented.

2 Materials and Methods

2.1 Brachytherapy source geometry and composition

The methods employed in this investigation characterizing a SPEC model M-15 HDR Iridium-192 brachytherapy source was similar to the methods used previously to dosimetrically characterize the SPEC model M-19 Iridium-192 source.⁸ The M-15 source was modeled in an MCNP6 Monte Carlo environment using the physical source specifications provided by the manufacturer. A graphical depiction of the M-15 used in the MC simulation is presented in Figure 1 with its corresponding physical parameters listed in Table 1. The source construction was symmetric about the coaxial axis but non-symmetric about the traverse plane due to the addition of an attached source cable.

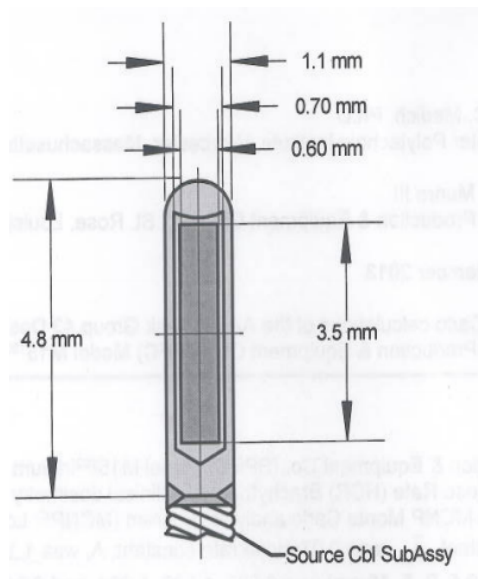


Figure 1: Configuration of the M-15 Iridium-192 HDR Brachytherapy source modeled for the MCNP simulation. This model consists of a 0.350cm long Iridium-192 source encapsulated in a steel shell

Table 1: Physical parameters of the M-15 Iridium-192 source used in the MCNP simulations

Component	Outside Diameter (mm)	Inside Diameter (mm)	Length (mm)	Density (mg/mm ³)	Remarks
Active	0.6	N.A	3.5	22.4	Iridium Metal
Encapsulation	1.1	0.7	4.8	7.8	Stainless Steel
Source Cable	1.1	N.A	2000	7.8	Stainless Steel

2.2 Monte Carlo calculation techniques

Radiation transport calculations were performed on a WindowsTM based personal computer running the MCNP6 Monte Carlo computer code.⁷ Iridium-192 photons were uniformly generated inside the iridium core of the Model M-15 with photon and secondary electron transport replicated using default MCPLIB04 photo-atomic cross-section tables supplied with MCNP6. Simulations were performed for both water and air/vacuum computer models with a total of 2×10^8 sources photon history for each simulation. All simulations were operated in the photon and electron transport mode (Mode: p,e in the MCNP code) so that both primary photons and resulting secondary electrons were properly transported.¹⁰ Iridium-192's photon spectrum¹¹ was simplified by disregarding photons with intensities below 0.1% and by omitting Iridium-192 source x-rays lower than 15 keV since transmission of these photons through the encapsulating steel shell is dosimetrically negligible. The resulting iridium spectrum used in this study and the uncertainty of each spectral line are presented in Table 2. The uncertainty in the spectrum, $\sigma_{I_\gamma}^{relative} = 0.5\%$, was calculated as the intensity weighted average of the uncertainty in each spectral line.

Dosimetric data, including $\dot{D}(r, \theta)$, $g_L(r)$, $F(r, \theta)$, $\phi_{an}(r)$, and $\bar{\phi}_{an}$, and their statistical uncertainty⁹ were calculated from the output of an MCNP computer model consisting of an M-15 source placed at the center of a spherical water phantom of 100 cm diameter; this diameter was chosen to approximate an infinite water phantom, allowing for full photon scattering conditions in the dosimetric regions of interest.^{10,12} Dosimetric data were calculated at radial distances ranging from 0.5 to 10 cm in half centimeter increments and over angles ranging from 0 deg to 180 deg using the MCNP6 F6 energy deposition tally, $R_{tally}(r, \theta)$, reported in units of MeV g⁻¹ photon⁻¹.

The energy deposition tally output, $R_{tally}(r, \theta)$, was multiplied by the Iridium-192 photon yield, $I_\gamma = 2.301\gamma Bq^{-1}s^{-1}$, to obtain the calculated dose deposited in the tally region per disintegration, $\dot{D}(r, \theta)$:

Table 2: Iridium-192 photon energy spectrum used in this study with the respective uncertainty in their photon yields (S.Y.F. Chu, L.P. Ekström, and R.B. Firestone, LBNL, Berkeley, CA, USA, 1999). Note that the relative uncertainties in the iridium-192 photon energies are insignificant when compared against the relative uncertainties in the photon yield. The total combined uncertainty in these data is expressed as a weighted average of the data with the photon intensity used as the weighting function

Energy (keV)	Intensity (%)	Uncertainty (%)
61.49	1.20	2.50
63.00	2.07	2.90
65.12	2.65	2.26
66.83	4.53	1.99
71.08	0.24	2.93
71.41	0.46	2.83
73.36	0.16	2.47
75.37	0.53	2.06
75.75	1.03	2.04
77.83	0.37	2.19
136.34	0.18	4.37
201.31	0.47	1.27
205.80	3.30	0.52
283.27	0.26	1.53
295.96	28.7	0.31
308.46	30.0	0.27
316.51	82.8	0.25
374.49	0.72	0.69
416.47	0.66	1.05
468.07	47.8	0.36
484.58	3.18	0.35
489.04	0.44	0.90
588.58	4.52	0.03
604.41	8.23	0.73
612.47	5.31	0.32
884.54	0.29	0.86
Total	230.12%	0.50%

$$\dot{D}(r, \theta) = R_{MonteCarlo}(r, \theta) I_\gamma \quad (1)$$

The result is expressed in units of $\text{MeV g}^{-1} \text{Bq}^{-1} \text{s}^{-1}$. From this, $\dot{D}(r, \theta)$ can be converted into more conventional units through the relationship: $1 \text{MeV g}^{-1} \text{Bq}^{-1} \text{s}^{-1} = 2.13 \times 10^3 \text{cGy mCi}^{-1} \text{h}^{-1}$.

The Air-Kerma strength in free space, K_k , was calculated using the methods described previously.⁸ The M-15 Iridium-192 source was centered at the origin of an evacuated phantom in which a critical volume containing air at STP was added 100cm from the source center. The MCNP6 *F4 tally (MeV/cm^2) output from the Air-Kerma simulation was multiplied by the respective air mass-energy absorption coefficient, μ_{en}/ρ (cm^2/g),¹³ to obtain the air kerma per source photon ($\text{MeV g}^{-1} \text{photon}^{-1}$). Equivalence is assumed between the air mass-energy transfer coefficient and the air mass-energy absorption coefficient due to negligible radiative energy losses.¹⁴ The x-ray cutoff energy, δ , was chosen to be $\delta = 10 \text{ keV}$; photons within the critical target with energies less than or equal to δ were removed from the final air kerma rate calculation. Once filtered, Air-Kerma strength in free space is found by multiplying the square of the source to volume distance by the resulting Air-Kerma rate.

3 Results and Discussion

3.1 Dose rate and normalized dose rate distribution

The Monte Carlo tally output $R_{tally}(r, \theta)$ at each point of interest in the water phantom is converted to the dose rate $\dot{D}(r, \theta)$ using equation (1). This dose rate correspond to the updated AAPM TG 43 dose rate in water:

$$\dot{D}_{TG-43}(r, \theta) = S_k \cdot \Lambda \cdot \frac{G(r, \theta)}{G(r_0, \theta_0)} \cdot F(r, \theta) \cdot g(r) \quad (2)$$

The absolute uncertainty in $\dot{D}(r, \theta)$ was calculated using the following equation:

$$\sigma_D^{absolute}(r, \theta) = \dot{D}(r, \theta) \sqrt{(\sigma_{MonteCarlo}^{relative}(r, \theta))^2 + (\sigma_{crosssection}^{relative})^2 + (\sigma_{I_\gamma}^{relative})^2} \quad (3)$$

These data were then corrected for the geometry effect by multiplying the dose rate, $\dot{D}(r, \theta)$, by the radial distance squared, r^{-2} . The resulting dose rate is then normalized to the reference dose in water, $\dot{D}(r_0, \theta_0) = 4.038 \pm 0.064 \text{ cGy mCi}^{-1} \text{ h}^{-1}$, to obtained $\dot{D}_N(r, \theta)$:

$$\dot{D}_N(r, \theta) = \frac{\dot{D}(r, \theta) \cdot r^2}{\dot{D}(r_0, \theta_0)} \quad (4)$$

A graphical representation of the normalized dose rate is presented in Figure 2. The tabular representation is also presented in Table 3 with the absolute uncertainty calculated using equation:

$$\sigma_{\dot{D}_N}^{absolute}(r, \theta) = \dot{D}_N(r, \theta) \sqrt{(\sigma_{MonteCarlo}^{relative}(r, \theta))^2 + (\sigma_{MonteCarlo}^{relative}(r_0, \theta_0))^2 + 2(\sigma_{crosssection}^{relative})^2} \quad (5)$$

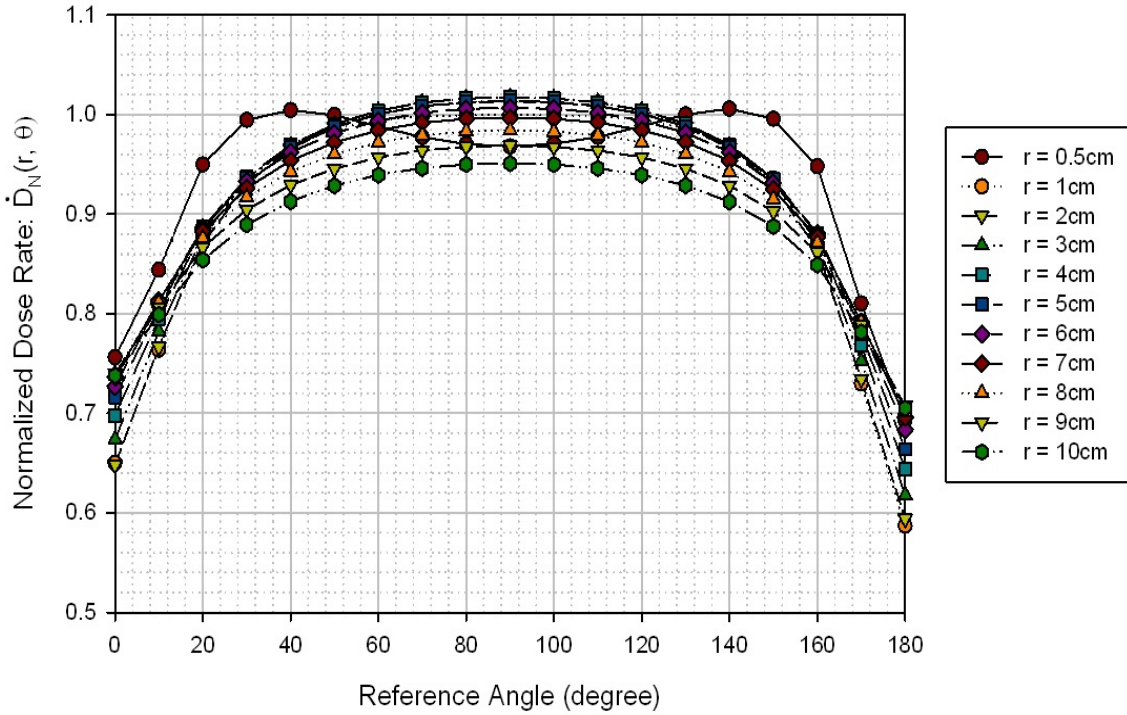


Figure 2: Presentation of the normalized dose rate distribution of model M-15 Iridium-192 from the MCNP output. Geometry effects were removed by multiplying the dose rate, $\dot{D}(r, \theta)$, by the radial distance squared, r^{-2} . Once corrected, the dose rate is then normalized to the dose rate at 1 cm along the seed's traverse's axis, $\dot{D}(r_0, \theta_0) = 4.038 \pm 0.064 \text{ cGy mCi}^{-1} \text{ h}^{-1}$, to obtain the normalized dose rate.

Table 3: Calculated normalized dose rate distribution of the M-15 Iridium-192 in water $\dot{D}_N(r, \theta) = [\dot{D}(r, \theta) \cdot r^2] / \dot{D}(r_0, \theta_0)$ with absolute uncertainty, $\sigma_{\dot{D}_N}$.

$\frac{r(\text{cm})}{\theta(^{\circ})}$	0.5	1	2	3	4	5	6	7	8	9	10
0	0.756 ± 0.016	0.65 ± 0.014	0.648 ± 0.014	0.674 ± 0.015	0.698 ± 0.015	0.716 ± 0.015	0.727 ± 0.016	0.736 ± 0.016	0.74 ± 0.016	0.74 ± 0.016	0.738 ± 0.016
10	0.844 ± 0.018	0.764 ± 0.016	0.767 ± 0.016	0.782 ± 0.017	0.795 ± 0.017	0.805 ± 0.017	0.811 ± 0.017	0.813 ± 0.017	0.811 ± 0.017	0.807 ± 0.017	0.799 ± 0.017
20	0.95 ± 0.020	0.875 ± 0.019	0.87 ± 0.018	0.878 ± 0.019	0.884 ± 0.019	0.887 ± 0.019	0.886 ± 0.019	0.883 ± 0.019	0.876 ± 0.019	0.866 ± 0.018	0.854 ± 0.018
30	0.995 ± 0.021	0.936 ± 0.020	0.93 ± 0.020	0.934 ± 0.020	0.937 ± 0.020	0.936 ± 0.020	0.933 ± 0.020	0.926 ± 0.020	0.917 ± 0.019	0.904 ± 0.019	0.89 ± 0.019
40	1.005 ± 0.021	0.968 ± 0.021	0.966 ± 0.020	0.969 ± 0.021	0.969 ± 0.021	0.967 ± 0.021	0.962 ± 0.020	0.954 ± 0.020	0.943 ± 0.020	0.929 ± 0.020	0.913 ± 0.019
50	0.999 ± 0.021	0.986 ± 0.021	0.987 ± 0.021	0.99 ± 0.021	0.99 ± 0.021	0.987 ± 0.021	0.981 ± 0.021	0.972 ± 0.021	0.96 ± 0.020	0.946 ± 0.020	0.929 ± 0.020
60	0.988 ± 0.021	0.994 ± 0.021	1.001 ± 0.021	1.004 ± 0.021	1.004 ± 0.021	1.000 ± 0.021	0.994 ± 0.021	0.984 ± 0.021	0.972 ± 0.021	0.957 ± 0.020	0.94 ± 0.020
70	0.977 ± 0.021	0.998 ± 0.021	1.008 ± 0.021	1.012 ± 0.021	1.012 ± 0.021	1.009 ± 0.021	1.002 ± 0.021	0.992 ± 0.021	0.979 ± 0.021	0.964 ± 0.020	0.946 ± 0.020
80	0.97 ± 0.021	0.999 ± 0.021	1.012 ± 0.021	1.016 ± 0.022	1.016 ± 0.022	1.013 ± 0.021	1.006 ± 0.021	0.996 ± 0.021	0.983 ± 0.021	0.968 ± 0.021	0.95 ± 0.020
90	0.968 ± 0.021	1.000	1.013 ± 0.021	1.017 ± 0.022	1.017 ± 0.022	1.014 ± 0.022	1.007 ± 0.021	0.997 ± 0.021	0.984 ± 0.021	0.969 ± 0.021	0.951 ± 0.020
100	0.971 ± 0.021	0.999 ± 0.021	1.012 ± 0.021	1.016 ± 0.022	1.016 ± 0.022	1.013 ± 0.021	1.006 ± 0.021	0.996 ± 0.021	0.983 ± 0.021	0.968 ± 0.021	0.95 ± 0.020
110	0.978 ± 0.021	0.999 ± 0.021	1.009 ± 0.021	1.012 ± 0.021	1.012 ± 0.021	1.009 ± 0.021	1.002 ± 0.021	0.992 ± 0.021	0.979 ± 0.021	0.964 ± 0.020	0.946 ± 0.020
120	0.989 ± 0.021	0.995 ± 0.021	1.001 ± 0.021	1.004 ± 0.021	1.004 ± 0.021	1.001 ± 0.021	0.994 ± 0.021	0.984 ± 0.021	0.972 ± 0.021	0.957 ± 0.020	0.94 ± 0.020
130	1.000 ± 0.021	0.987 ± 0.021	0.988 ± 0.021	0.991 ± 0.021	0.991 ± 0.021	0.988 ± 0.021	0.982 ± 0.021	0.972 ± 0.021	0.96 ± 0.020	0.946 ± 0.020	0.929 ± 0.020
140	1.006 ± 0.021	0.969 ± 0.021	0.966 ± 0.020	0.969 ± 0.021	0.97 ± 0.021	0.967 ± 0.021	0.962 ± 0.020	0.954 ± 0.020	0.943 ± 0.020	0.929 ± 0.020	0.913 ± 0.019
150	0.996 ± 0.021	0.936 ± 0.020	0.929 ± 0.020	0.933 ± 0.020	0.935 ± 0.020	0.935 ± 0.020	0.931 ± 0.020	0.925 ± 0.020	0.915 ± 0.019	0.903 ± 0.019	0.888 ± 0.019
160	0.948 ± 0.020	0.87 ± 0.018	0.864 ± 0.018	0.872 ± 0.018	0.878 ± 0.019	0.881 ± 0.019	0.881 ± 0.019	0.877 ± 0.019	0.871 ± 0.018	0.861 ± 0.018	0.849 ± 0.018
170	0.81 ± 0.017	0.73 ± 0.015	0.734 ± 0.016	0.752 ± 0.016	0.768 ± 0.016	0.78 ± 0.017	0.788 ± 0.017	0.792 ± 0.017	0.792 ± 0.017	0.788 ± 0.017	0.782 ± 0.017
180	0.692 ± 0.015	0.587 ± 0.013	0.594 ± 0.013	0.618 ± 0.013	0.644 ± 0.014	0.664 ± 0.014	0.684 ± 0.015	0.696 ± 0.015	0.702 ± 0.015	0.708 ± 0.015	0.705 ± 0.015

3.2 Geometry function, $G_L(r, \theta)$

The geometry function, $G_L(r, \theta)$, accounting for the spatial distribution of radioactivity within the source, was calculated using the TG43U1 approximation for a line source of length L and subtended angle β :

$$G_L(r, \theta) = \frac{\beta}{Lr \sin(\theta)} \quad (6)$$

The value of L for M-15 Iridium-192 source is 0.350cm. Results are represented in Table ? and Figure ?.

3.3 Radial dose function, $g_L(r)$

The radial dose function $g_L(r, \theta)$ of model M-15 Iridium 192, a geometry independent dosimetric parameter accounting for dose fall-off on traverse-plane due to photon scattering and attenuation, was calculated using the TG43U1 formalism:

$$g_L(r) = \frac{\dot{D}(r, \theta_0) G_L(r_0, \theta_0)}{\dot{D}(r_0, \theta_0) G_L(r, \theta_0)} \quad (7)$$

The radial dose function was computed for radial distance from 0.25 cm to 15 cm. The absolute uncertainty $g_L(r, \theta)$ was also computed using Eq ?:

$$\sigma_{g_L}^{absolute}(r) = g_L(r) \sqrt{(\sigma_{MonteCarlo}^{relative}(r, \theta_0))^2 + (\sigma_{MonteCarlo}^{relative}(r_0, \theta_0))^2 + 2(\sigma_{crosssection}^{relative})^2} \quad (8)$$

The results are presented in Table 4. For clinical implementation, these results were fit to a 5th order polynomial. As the polynomial fitting function is unreliable outside the distances used in the regression analysis, a double exponential fit of the form: $g_L(r) = C_1 \cdot e^{\mu_1 \cdot r} + C_2 \cdot e^{\mu_2 \cdot r}$ has also been performed. The resulting 5th order polynomial coefficients and the double exponential coefficients are presented in Table 5. Graphical presentation of the computed results and regression coefficients are presented in Figure 3.

Table 4: Calculated radial dose function, $g_L(r)$, for the M-15 Iridium-192 source with the absolute uncertainty, $\sigma_{g_L}(r)$.

r (cm)	$g_L(r)$	$\sigma_{g_L}(r)$
0.5	0.996	0.021
1.0	1.00	0
2.0	1.006	0.021
3.0	1.008	0.021
4.0	1.008	0.021
5.0	1.004	0.021
6.0	0.997	0.021
7.0	0.987	0.021
8.0	0.974	0.021
9.0	0.959	0.020
10.0	0.941	0.020

Table 5: Summary of the fifth order polynomial regression coefficients and double exponential regression for the M-15 Iridium-192 radial dose function. For treatment planning, the radial dose function at $r = 0$ should be derived from the double exponential fit resulting in $g_L(0) = 0.994$.

Fifth order polynomial parameters	Fifth order polynomial coefficients	Double exponential parameters	Double exponential coefficients
a_0	0.9919	C_1	-0.08651
a_1	0.0092	μ_1	0.1312
a_2	-0.0009	C_2	1.081
a_3	-0.0001	μ_2	0.01549
a_4	1.29×10^{-5}		
a_5	3.74×10^{-7}		

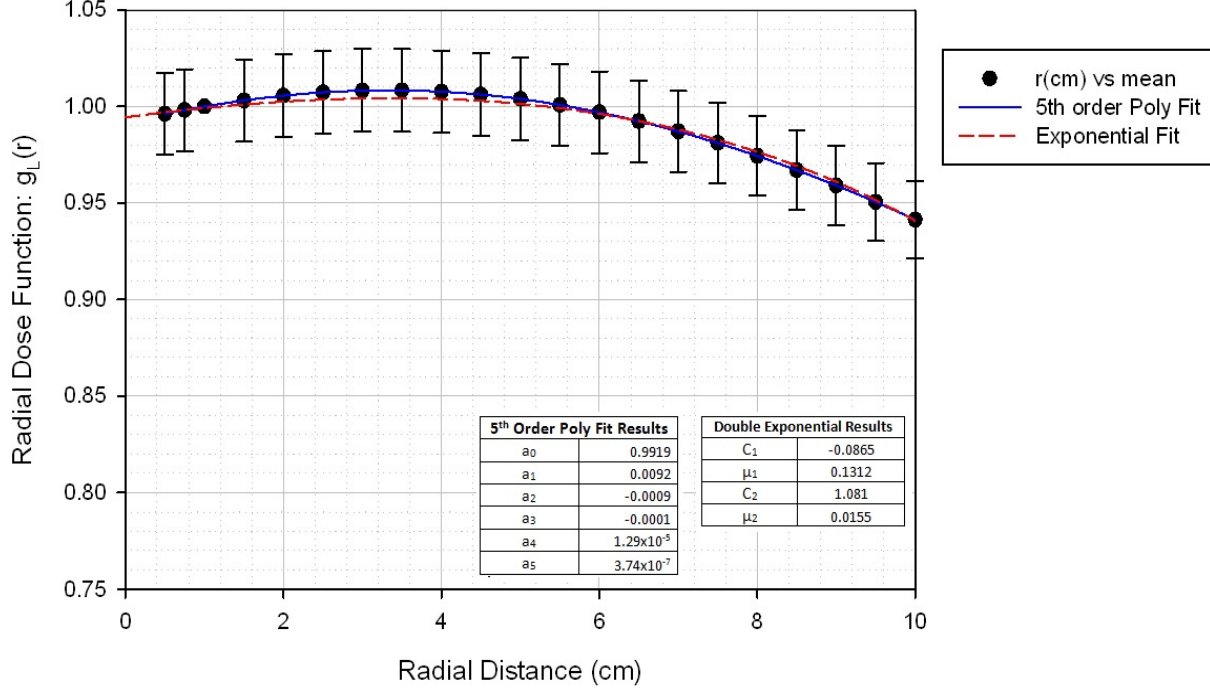


Figure 3: Calculated M-15 radial dose function, $g_L(r)$, at distance between 0.5 and 10cm with the resulting data fit to a fifth order polynomial and double exponential function

3.4 Anisotropy Function, $F(r, \theta)$, $\phi_{an}(r)$, and $\bar{\phi}_{an}$

The anisotropy function, $F(r, \theta)$ was calculated using the TG43U1 equation:

$$F(r, \theta) = \frac{\dot{D}(r, \theta) G_L(r, \theta_0)}{\dot{D}(r, \theta_0) G_L(r, \theta)} \quad (9)$$

The uncertainty in the anisotropy function, $F(r, \theta)$ was calculated using equation:

$$\sigma_F^{absolute}(r, \theta) = F(r, \theta) \sqrt{(\sigma_{MonteCarlo}^{relative}(r, \theta))^2 + (\sigma_{MonteCarlo}^{relative}(r_0, \theta_0))^2 + 2(\sigma_{crosssection}^{relative})^2} \quad (10)$$

The result are presented in Table 6.

Table 6: Calculated anisotropy function, $F(r, \theta)$, and anisotropy factor, $\phi_{an}(r)$, and their absolute uncertainties for M-15 Iridium-192

$\frac{r \text{ (cm)}}{\theta(^{\circ})}$	0.5	1	2	3	4	5	6	7	8	9	10
0	0.66	0.624	0.633	0.659	0.684	0.705	0.721	0.738	0.751	0.763	0.776
	± 0.014	± 0.014	0.014	± 0.014	± 0.015	± 0.015	± 0.016	± 0.016	± 0.016	± 0.016	± 0.017
10	0.74	0.734	0.749	0.765	0.78	0.793	0.804	0.815	0.824	0.832	0.84
	± 0.016	± 0.016	± 0.016	± 0.016	± 0.017	± 0.018	± 0.018				
20	0.848	0.844	0.851	0.859	0.867	0.874	0.879	0.885	0.889	0.894	0.898
	± 0.018	± 0.019									
30	0.911	0.908	0.911	0.915	0.919	0.923	0.926	0.929	0.931	0.933	0.935
	± 0.019	± 0.019	± 0.019	± 0.019	± 0.020						
40	0.948	0.946	0.947	0.95	0.951	0.953	0.955	0.956	0.958	0.959	0.96
	± 0.020										
50	0.971	0.97	0.97	0.971	0.972	0.973	0.974	0.975	0.975	0.976	0.976
	± 0.021										
60	0.985	0.984	0.985	0.986	0.986	0.987	0.987	0.987	0.988	0.988	0.988
	± 0.021										
70	0.993	0.994	0.994	0.994	0.995	0.995	0.995	0.995	0.995	0.995	0.995
	± 0.021										
80	0.998	0.998	0.999	0.999	0.999	0.999	0.999	0.999	0.999	0.999	0.999
	± 0.021										
90	1.000	1.000	1.000	1.000	1.000	1.000	1.000	1.000	1.000	1.000	1.000
	0.998	0.998	0.999	0.999	0.999	0.999	0.999	0.999	0.999	0.999	0.999
100	± 0.021										
	0.993	0.994	0.994	0.995	0.995	0.995	0.995	0.995	0.995	0.995	0.995
110	± 0.021										
	0.985	0.985	0.986	0.986	0.987	0.987	0.987	0.987	0.988	0.988	0.988
120	± 0.021										
	0.972	0.97	0.971	0.972	0.973	0.974	0.974	0.975	0.976	0.976	0.977
130	± 0.021										
	0.949	0.947	0.948	0.95	0.952	0.953	0.955	0.956	0.957	0.958	0.959
140	± 0.020										
	0.913	0.908	0.91	0.914	0.918	0.921	0.924	0.927	0.929	0.932	0.933
150	± 0.019	± 0.020									
	0.847	0.839	0.845	0.853	0.861	0.868	0.874	0.88	0.885	0.889	0.893
160	± 0.018	± 0.019									
	0.711	0.701	0.718	0.736	0.753	0.768	0.782	0.793	0.804	0.814	0.822
170	± 0.015	± 0.015	± 0.015	± 0.016	± 0.016	± 0.016	± 0.017				
	0.604	0.563	0.58	0.604	0.632	0.654	0.678	0.698	0.713	0.73	0.741
180	± 0.013	± 0.012	± 0.013	± 0.013	± 0.014	± 0.014	± 0.015	± 0.015	± 0.015	± 0.016	± 0.016
	1.009	0.971	0.963	0.964	0.965	0.966	0.967	0.968	0.969	0.97	0.971
$\phi_{an}(r)$	± 0.015	± 0.014									

The anisotropy factor, $\phi(r)$ was also calculated using the formula:

$$\phi_{an}(r) = \frac{\int_0^\pi \dot{D}(r, \theta) \sin(\theta) d\theta}{2\dot{D}(r, \theta_0)} \quad (11)$$

The absolute uncertainty in $\phi(r)$ was calculated as:

$$(\sigma_{\phi_{an}}^{absolute})^2(r) = \left[\phi_{an}(r) - \frac{\Delta\theta}{2} \right]^2 [\sigma_{Rtally}^{relative}(r, \theta_0)]^2 + \sum_{\substack{\theta=0 \\ \theta \neq \theta_0}}^{\pi} \left[\left(\frac{\dot{D}(r, \theta)}{\dot{D}(r, \theta_0)} \frac{\sin(\theta)}{2} \Delta\theta \right)^2 [\sigma_{Rtally}^{relative}(r, \theta)]^2 \right] \quad (12)$$

The result are also presented in Table 6 for the radial distance from $0.5cm$ to $10cm$. From this data, the anisotropy constant was calculated to be $\bar{\phi}_{an} = 0.969 \pm 0.007$ by integrating $\phi_{an}(r)$ between $1cm$ and $10cm$ using the weighting factor proportional to r^{-2} . The absolute uncertainty in $\bar{\phi}_{an}$ was calculated using equation:

$$(\sigma_{\bar{\phi}_{an}}^{absolute})^2 = \sum_{r=1}^{10} [w(r)\Delta r]^2 \sigma_{\phi_{an}}^2(r) \quad (13)$$

3.5 $\dot{D}(r_0, \theta_0)$, S_k , and Λ

The Monte Carlo calculated reference dose rate in water $\dot{D}(r_0, \theta_0) \equiv \dot{D}(1cm, \pi/2)$, was determined to be $\dot{D}(r_0, \theta_0) = 4.038 \pm 0.064 \text{ cGy } mCi^{-1} h^{-1}$. The absolute uncertainty in $\dot{D}(r_0, \theta_0)$ was calculated using equation (3).

The Air-Kerma in free space, S_k was reported to be $S_k = 3.632 \mu \text{ cGy } cm^2 mCi^{-1} g^{-1}$. The absolute uncertainty in S_k was calculated to be $\sigma_{S_k}^{absolute} = 0.086 \text{ cGy } cm^2 mCi^{-1} h^{-1}$ using the following equation:

$$\sigma_{S_k}^{absolute} = S_k \sqrt{(\sigma_{MonteCarlo}^{relative})^2 + (\sigma_{crosssection}^{relative})^2 + (\sigma_{I_\gamma}^{relative})^2} \quad (14)$$

From the above data, the dose rate constant can be calculated using:

$$\Lambda = \frac{\dot{D}(r_0, \theta_0)}{S_k} \quad (15)$$

The reported dose rate constant Λ is $\Lambda = 1.112 \text{ cGy } h^{-1} U^{-1}$. The absolute uncertainty has been calculated to be using the following $\sigma_{\Lambda}^{absolute} = 0.029 \text{ cGy } h^{-1} U^{-1}$ using the following equation:

$$\sigma_{\Lambda}^{absolute} = \Lambda \sqrt{(\sigma_{Rtally}^{relative}(r_0, \theta_0))^2 + (\sigma_{P^{10}^{air-Kerma}}^{relative})^2} \quad (16)$$

4 Conclusions

A dosimetric study of the M-15 iridium-192 HDR brachytherapy source was performed using the MCNP6 radiation transport code. The dose rate constant, radial dose function, anisotropy function were calculated in accordance with the updated AAPM Technical Guidance Document 43. These data may be applied towards clinical use and towards the development of a treatment program.

References

- [1] Subir Nag, "High dose rate brachytherapy: Its clinical applications and treatment guidelines," *Technol. Cancer Res. Treat.* **3**, 269-287 (2004).
- [2] K. S. Kapp, G. F. Stueckelschweiger, D. S. Kapp, J. Poschauko, H. Pickel, and A Hackl, "Carcinoma of the cervix: Analysis of complications after primary external beam radiation and Ir-192 HDR brachytherapy," *Radiother. Oncol.* **42**, 143-153 (1997).
- [3] J. Hammer, D. H. Seewald, C. Track, J. P. Zoidl, and W. Labeck, "Breast cancer: Primary treatment with external-beam radiation therapy and high-dose-rate iridium implantation," *Radiology* **193**, 573-577 (1994).
- [4] R. Schmidt-Ullrich, R. D. Zwicker, A. Wu, and K. Kelly, "Interstitial Ir-192 implants of the oral cavity: The planning and construction of volume implants," *Int. J. Radiat. Oncol., Biol., Phys.* **20**, 1079-1085 (1991).
- [5] K. S. Kapp, G.F. Stueckelschweiger, D. S. Kapp, J. Poschauko, H. Pickel, M. Lahousen, and A. Hackl "Prognostic factors in patients with carcinoma of the uterine cervix treated with external beam irradiation and Ir-192 high-dose-rate brachytherapy," *Int. J. Radiat. Oncol., Biol., Phys.* **42**, 531-540 (1998).
- [6] M. J. Rivard, B.M. Coursey, L. A. DeWerd, W. F. Hanson, M. S. Huq, G. S. Ibbott, M. G. Mitch, R. Natt, and J. F. Williamson, "Updated AAPM Task Group No. 43 Report: A revised AAPM protocol for brachytherapy dose calculations," *Med. Phys.* **31**, 633-674 (2004).
- [7] Thomas E. Booth *et al.*, "MCNP - A general Monte Carlo N-particle transport code, Version 5," Report No. LA-UR-03-1987, 2003.
- [8] David C. Medich, and John J. Munro III "Monte Carlo characterization of the M-19 high dose rate Iridium-192 brachytherapy source," *Med. Phys.* **34**, 1999-2006 (2007).

- [9] David C. Medich, M. A. Tries, and John J. Munro III "Monte Carlo characterization of an ytterbium-169 high dose rate brachytherapy source with analysis of statistical uncertainty," *Med. Phys.* **33**, 163-172 (2006).
- [10] C. S. Melthus and M. J. Rivard, "Approaches to calculating AAPM TG-43 brachytherapy dosimetry parameters for ^{137}Cs , ^{125}I , ^{192}Ir , ^{103}Pd , and ^{169}Yb sources," *Med. Phys.* **33**, 1729-1737 (2006).
- [11] S. Y. F. Chu, L. P. Ekström, and R. B. Firestone, The Lund/LBNL Nuclear Data Search, database version 1999-02-28 <http://nucleardata.nuclear.lu.se/nucleardata/toi/index.asp>, 1999.
- [12] J. Perez-Calatayud, D. Granero, and F. Ballester, "Phantom size in brachytherapy source dosimetric studies," *Med. Phys.* **31**, 2075-2081 (2004).
- [13] J. H. Hubbell and S. M. Seltzer, Tables of x-ray mass attenuation coefficients and mass energy absorption coefficients (version 1.03), <http://physics.nist.gov/PhysRefData/XrayMassCoef/cover.html>, 1997.
- [14] M. J. Berger, J. S. Coursey, and M. A. Zucker, Stopping-Power and Range Tables for Electrons, Protons, and Helium Ions, <http://physics.nist.gov/PhysRefData/Star/Text/contents.html>, 2000.